photonics

MDPI

Article

Extra-High Pressure in the Core of Silica-Based Optical Fiber Preforms during the Manufacturing Process

Galina Bufetova [1,*], Alexey Kosolapov [2], Mikhail Yashkov [3], Andrey Umnikov [3], Vladimir Velmiskin [2], Vladimir Tsvetkov [1] and Igor Bufetov [2]

[1] Prokhorov General Physics Institute of the Russian Academy of Sciences, 119991 Moscow, Russia
[2] Prokhorov General Physics Institute of the Russian Academy of Sciences, Dianov Fiber Optics Research Center, 119333 Moscow, Russia
[3] Institute of Chemistry of High-Purity Substances of the Russian Academy of Sciences, 603951 Nizhny Novgorod, Russia
* Correspondence: bufetova@lsk.gpi.ru

Abstract: The core refractive index n_2 of silica-based optical fiber preform heated to 2000 °C was determined experimentally for the first time. The measurements were carried out in the process of preform temperature reduction. It was shown that n_2 could increase up to ~1.75 in the visible spectral range at temperatures of ~2000 °C ($n_2 \approx 1.46$ at room temperature). This fact suggests that pressures close to or exceeding the ultimate strength of silica glass (~20 GPa) occur in the preform core region. The local extra pressure is argued to be a possible cause of the well-known "starburst" phenomenon at the core–cladding interface of preforms with certain core compositions. The observed effect of radial cracks can be interpreted as the result of silica cladding destruction under the action of extra-high pressure in the core.

Keywords: MCVD technology; FCVD technology; core–cladding interface; refractive index of core; silica glass; "starbursts" in fiber preforms

Citation: Bufetova, G.; Kosolapov, A.; Yashkov, M.; Umnikov, A.; Velmiskin, V.; Tsvetkov, V.; Bufetov, I. Extra-High Pressure in the Core of Silica-Based Optical Fiber Preforms during the Manufacturing Process. *Photonics* **2023**, *10*, 335. https://doi.org/10.3390/photonics10030335

Received: 26 December 2022
Revised: 16 March 2023
Accepted: 19 March 2023
Published: 21 March 2023

1. Introduction

The properties of glasses depend, to a large extent, on their fabrication conditions and heat treatment prehistory, even though the glass composition remains the same. The best-known example here appears to be the difference between tempered glass and the same glass that was not heat-treated [1,2]. In fact, preforms of optical silica-based fibers usually consist of glasses that differ in their composition. Specifically, core and cladding glasses are usually different in terms of optical and physical parameters, such as coefficient of thermal expansion (CTE), glass transition temperature (T_g), refractive index (RI), and optical loss [3–5].

During the preform fabrication process and during subsequent fiber drawing, the glass temperature varies over a rather wide range (from ~2000 °C to room temperature). Obviously, the properties of the core and cladding glasses can change in different ways during the treatment processes.

The cladding usually consists of pure silica glass, which has a low CTE up to the glass transition temperature T_g [4]. The CTE difference of the core and the cladding glasses can cause mechanical stresses in preforms and fibers. These can be both residual stresses, i.e., stresses remaining in preforms and fibers after cooling to room temperature, and stresses arising during the manufacturing process at high temperatures. Residual mechanical stresses in preforms and fibers have been studied profoundly (see, e.g., the review in [6] and references therein). In particular, this effect is widely used in polarization-maintaining fibers, e.g., in panda-type fibers. At the same time, the preform properties immediately during fabrication at high temperatures have been studied to a lesser extent, to the best of authors' knowledge and belief.

In particular, until now, there have been no studies measuring the core glass RI directly during fabrication (at temperatures of about 2000 °C and over), apparently owing to the complexity of such measurements. However, recently, a relatively simple method was proposed for determining the RI at the interface between two media with different RI, which is applicable at high temperatures. The method is based on comparing the intensities of intrinsic thermal radiation of a partially transparent sample in two perpendicular linear polarizations [7]. Thermal radiation is used in this method as the probing radiation. It was shown that, under certain conditions, the difference in radiation intensities for the angular diagrams of two polarizations reaches a maximum that can be denoted as $Q(n)$. The $Q(n)$-value is almost a linear function of the relative RI of the contacting media ($n = n_2/n_1$); by obtaining the $Q(n)$-value, the refractive index n can be determined. This method was used to determine the RI of sapphire and garnet crystal fibers at high temperatures (above 2000 K) directly in the process of their growth [8]. In fact, the same method can also be used to determine the core RI in the process of silica fiber preform fabrication. Additional data on preform behavior during the manufacturing process can provide new opportunities for controlling the process.

In this work, using the above optical method, the RI of the core glass melt of an optical fiber preform was determined. The measurements were performed when a preform was treated in the furnace chemical vapor deposition (FCVD) lathe. On the basis of the RI values obtained, the pressure in the core region during the preform cooling was estimated.

2. Experimental Setup and Samples

The setup for registration of angular patterns of the thermal radiation intensity from a heated silica preform is shown in Figure 1. Fiber preforms were heated in the FCVD lathe. The angular distributions of the thermal radiation intensity of the preform in mutually perpendicular polarizations were measured on the basis of the acquisition of optical images of the heated preform (Figure 1a). The images were formed by paraxial beams of the thermal radiation in the P- and S-polarizations (where the electric field direction is parallel or perpendicular to the plane of incidence, respectively) of the visible radiation using a telescopic system as depicted in Figure 1b. A linear polarizer in the P- or S-direction (2) was placed in front of the telescopic system (3). A λ/4 plate was used to compensate for the polarization sensitivity of the recording equipment. The distance from the preform to the camera was ~150 cm. The diameter of the diaphragm before the telescope was 4 mm. Thus, the image was formed by beams deviating from the axis by less than 0.2°. The image was formed on a photosensitive matrix of the camera (4). The exposure time was 1/8 s. During exposure, the preform rotated by 30° in the lathe (i.e., the rotation speed was 40 rpm); therefore, the obtained images were averaged within the rotation angle. The $I_p(x)$ and $I_s(x)$ profiles were determined from digital images (in grayscale) captured by the camera, where x is the coordinate of the distribution of S- and P-polarization intensity across the preform.

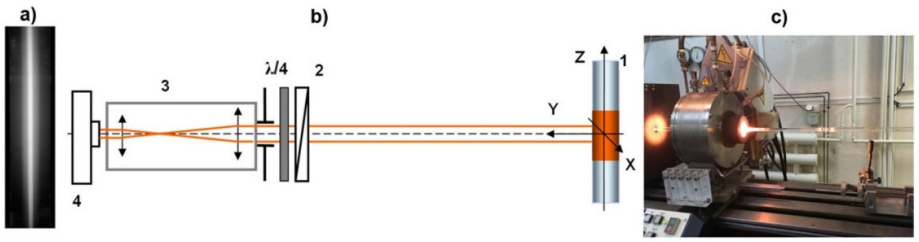

Figure 1. (**a**) The captured image of the heated part of the preform; (**b**) experimental setup (schematic view from the top). In the diagram, the numbered elements are as follows: the preform (1) is located along the horizontal axis Z, the polarizer (2) and λ/4 plate are placed in front of the telescope (3), and the image is formed on the matrix of the camera (4); (**c**) The main view of the FCVD lathe with heated preform.

The preform under investigation was placed inside the induction furnace of the FCVD lathe and was heated while being rotated for 1 min (Figure 1c). The temperature in the furnace was measured using an optical pyrometer. The heated section of the preform was secured inside the furnace body, surrounded by a graphite heating element and a metal casing; hence, it was not directly accessible for the optical measurements. Therefore, the graphite furnace was moved (at a velocity of ~3 cm/s) along the axis of the lathe immediately before starting the measurements, opening the heated area of the preform for the image acquisition. The imaging system was switched on at the same time.

We used in these measurements two silica preforms with different core compositions. Both preforms were fabricated by the modified chemical vapor deposition (MCVD) method (MCVD and FCVD methods are very similar [9]). These preforms were (1) the preform with a phosphosilicate core (PS) doped with ~6 mol.% P_2O_5, and (2) the preform with a germanosilicate core (GS) doped with ~23 mol.% GeO_2. The GS preform was made with several inner-cladding silica glass layers. Silica reference tubes (F-300 Heraeus) were used in the process of manufacturing the preforms. Series of measurements were carried out at the same temperature and time duration of the preform heating in the furnace. Figure 2 shows pictures of the cores of PS and GS preforms at room temperature, with a side view (a) and a cross-section view (b). RI profiles of preforms are depicted in Figure 2c.

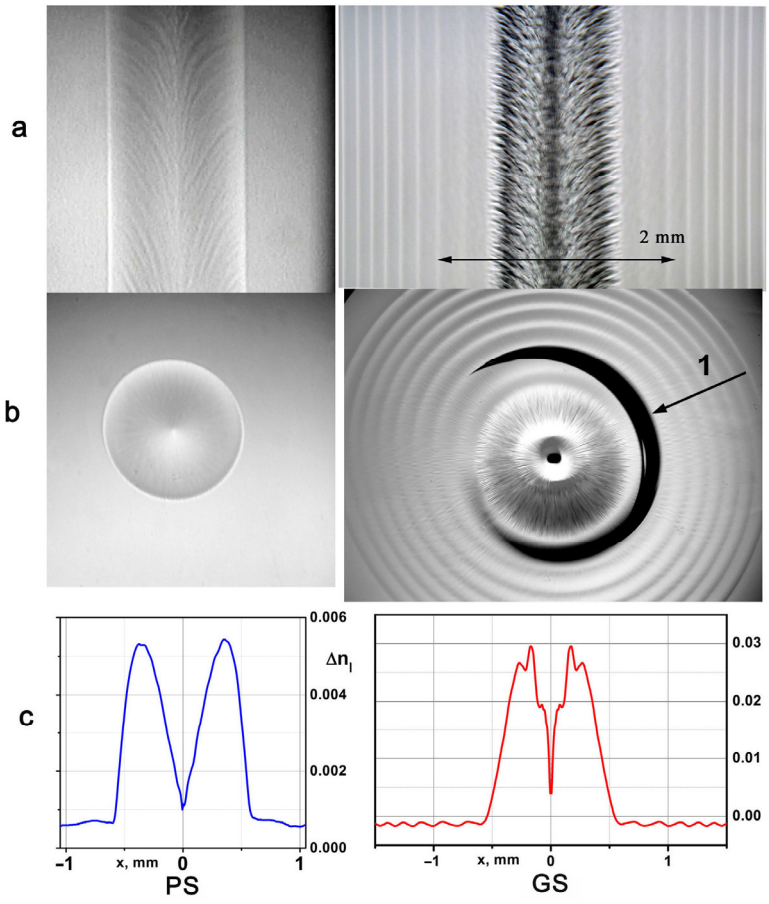

Figure 2. (PS) The PS preform data: (**a**) picture of the smooth core–cladding interface taken in the direction perpendicular to the preform axis; (**b**) a cross-section of the preform with core in the center; (**c**) RI profile of the PS preform. (GS) The GS preform data: (**a**) picture of the "hedgehog" shape of core–cladding interface taken in the direction perpendicular to the preform axis; (**b**) a cross-section view with "star" and an annular crack around the core (**1**), formed during the processing of a cross-sectional specimen. (**c**) RI profile of the GS preform. The linear scale is the same for all pictures and is shown in the GS photo (**a**). Side-view pictures (**a**) were taken using immersion.

The diameter of the PS preform was D = 11.5 mm, while the diameter of the core was d = 1.1 mm. Small inhomogeneities along the core of the preform are noticeable in Figure 2a (PS). In general, the images in Figure 2a,b (PS) were low-contrast, since RI gradients were not very high.

The pictures and RI profile of the GS preform with a relatively high level of Ge dopant are shown in Figure 2a–c (GS). The diameter of the preform with the GS core was D = 12.5 mm, while the diameter of the doped core was d = 1.0 mm. At room temperature, the shapes of the GS core and PS core of these two preforms differed noticeably. In the cross-section of the GS preform, depicted in Figure 2b (GS), the typical "starburst" can be seen [10,11]. The side view in Figure 2a (GS) shows that the core–cladding interface in the GS preform had a complicated "hedgehog" structure.

The rays of this "star" shape appeared very similar to radial cracks in the cladding. When cutting the GS preform at room temperature (or "cold" preform) with a diamond disc in the process of sample preparation, an annular crack appeared in the area close to the core. In fact, in Figure 2b (GS), one can see radial rays, formed during the process of manufacturing of the preform, as well as an annular crack (**1**) that occurred when cutting the "cold" preform. The RI profiles of both preforms (Figure 2c (PS and GS)) had a dip in the center. This sort of "dip" in the profile is typical for preforms manufactured by the MCVD process with volatile oxides as core dopants.

3. Measurements of the Profile of Thermal Radiation Intensity of the Preforms at a Temperature of T = 2000 °C

The intensity of thermal radiation of the heated PS and GS preforms was captured according to the scheme shown in Figure 1. Photographs of the heated area of the preforms and their intensity profiles of intrinsic thermal radiation are depicted in Figure 3.

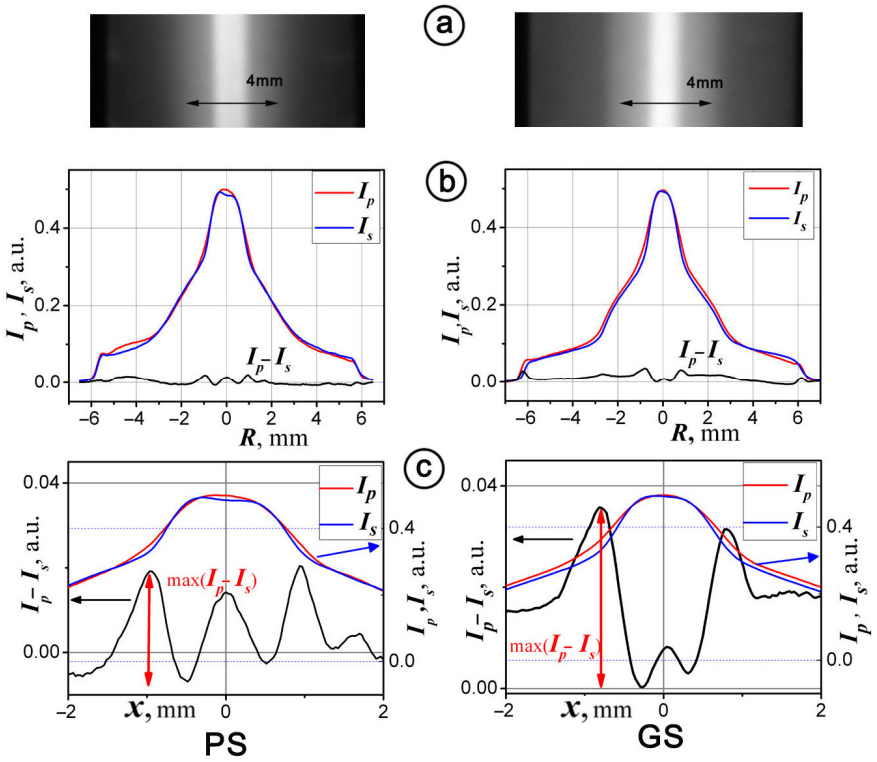

Figure 3. (PS) The PS preform data and (GS) the GS preform data: (**a**) image of the heated region of the preform; (**b**) measured intensity of the thermal radiation (in the visible range) for two polarizations against the x-coordinate, where $I_p(x)$ is marked by a red line and $I_s(x)$ is marked by a blue line; (**c**) center region of the preform (−2 mm < x < 2 mm).

First of all, we consider the results of measurements for the PS preform. When the preform was heated (up to T = 2000 °C) and appeared from the furnace, its core glowed brightly (Figure 3a (PS)). The radiation intensity of the cladding near the core was essentially less than that of the core. The radiation intensity of the cladding decreased toward the edges due to cooling. Figure 3b (PS) shows the distribution profiles of the thermal radiation intensity of the preform, for both polarizations $I_p(x)$ and $I_s(x)$, as well as their difference $I_p(x) - I_s(x)$.

The polarization intensity profiles $I_p(x)$ and $I_s(x)$ differed from each other (Figure 3b,c (PS)). The difference between $I_p(x)$ and $I_s(x)$ have apparent local maxima at the core–cladding interface (Figure 3c (PS)). The maximal value of the $Q(n) = max_x(I_p(x,n) - I_s(x,n))$ difference was about 4% of $I_p(x = 0)$. The x coordinate for the $Q(n)$ was close to the core radius. The heat radiation revealed the presence of a core–cladding interface. Using the method described in [7,8], we determined the relative refractive index corresponding to this value of $Q(n)$.The relative value of RI for the PS preform turned out to be $n_2/n_1 = 1.12$. The RI of the core was n_2, while the RI of the cladding was n_1.

It was also possible to estimate the RI of the heated preform cladding from its image. In Figure 3, the size of the core image was increased by n_1 times, since the cladding functioned as a cylindrical glass lens. A comparison of the core size in Figures 2 and 3 allowed us to evaluate the RI of the cladding as $n_1 = 1.47 \pm 0.01$. The value of the refractive index with the best fit was $n_2 = 1.64 \pm 0.01$. The accuracy of n_2 was determined from the rms deviation of the calculated and measured profile of $I_p(x,n) - I_s(x,n)$ [7].

Next, we consider the thermal radiation of the GS preform and compare it with that of the PS preform. The observed maxima $Q(n) = max_x(I_p(x,n) - I_s(x,n))$ at the interface of both media for GS and PS were similar in shape, but differed in magnitude. It is necessary to underline that despite the complicated form of the interface between the GS core and its cladding, the thermal "probing" radiation demonstrated difference in intensity between P- and S-polarizations even in this case. The maximum value of $Q(n)$ for the GS preform was 7% of $I_p(x = 0)$, corresponding to $n_2/n_1 = 1.19$ (where $n_2 = 1.75 \pm 0.01$) according to a lower estimation. The core values of RI obtained even from a lower estimation were very high for both preforms. To estimate the RI, we compared the maximum observed values of $Q(n)$ with the calculated ones. Simulations with the use of Fresnel formulas were performed for the interface between core and cladding with different RI (n_2 and n_1). However, in performed calculations, the effect on the peak value $Q(n)$ of the preform rotation and, in the case of the GS preform, the complex shape of the interface were not taken into account. These are additional reasons for the broadening of the observed maxima of $Q(n)$. When the preform was rotated, the interface line of the two media was shifted in the image plane and could give a wider integral peak of a lower amplitude. Therefore, we obtained a lower estimation for the RI values.

It is known that the RI of silica glass depends significantly on pressure; for example, it reaches a value of 1.9 when the pressure increases to 60 GPa [12]. Therefore, a high value of the core RI can actually originate from the high pressure in the core material. The obtained values of n_2 correspond to a pressure in the molten core of more than 15 GPa for the PS preform and even more than 30 GPa for the GS preform (if we use the data in [12] as an initial approximation for estimation).

4. Discussion of the Results

The divergence in the intensity of mutually orthogonal linear polarizations may indicate a significant difference in the RI of the material of the core n_2 and the cladding n_1 (provided that the Fresnel formulas are valid at the core–cladding interface). The corresponding difference in the RI was estimated as $\Delta n = n_2 - n_1 \approx 0.2$–$0.3$.

Therefore, high values of Δn can hardly be explained other than by a significant compression of the core material. The high pressure in the molten core generates tensile stress in the adjacent solidified cladding. The magnitude of the tensile stress of the inner layer of the cladding in the annular direction is equal to the pressure in the core [13]. If

the tensile stress in the cladding exceeds the failure threshold value, then cracks appear in the cladding. The tensile stress failure threshold of pure silica glass can be theoretically estimated as several tens of GPa (e.g., 13 GPa in [14] or 32 GPa in [15]). The maximal experimental value of the failure threshold of silica glass (18 GPa) was obtained for silica fibers in [16,17].

Tensile stresses in preforms can lead to their failure through crack propagation (for example, as in the case of tempered glass). Residual stresses at room temperature in the MCVD preform core are mainly tensile [6,18]. Of the various types of MCVD preforms fabricated by us, the highest residual stresses were exhibited by borosilicate (BS) preforms with a core doped with 20 mol.% B_2O_3 (Figure 4a–c). These were preforms for stress elements in panda-type fibers and did not differ in manufacturing technology from conventional preforms for silica fibers.

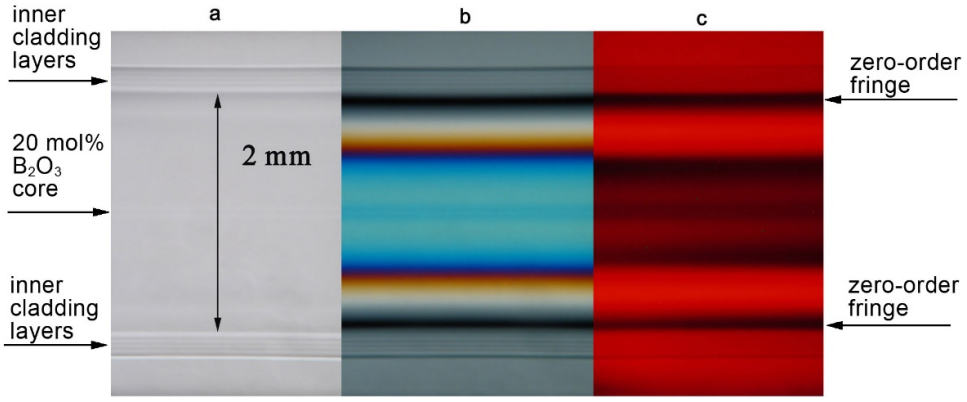

Figure 4. Photographs of the BS preform (for stress elements in panda-type fibers) taken in various conditions with the use of an optical microscope. Side view. (**a**) Transmitted white light optical image. Inner cladding layers are visible. (**b**) Transmitted white light optical image with crossed polarizers. Qualitative picture of stresses in the core. (**c**) Transmitted red light optical image with crossed polarizers. At the center of the core, the phase difference is about ~1.5 fringes.

A tensile stress of 0.05 GPa was observed in the core of the BS preform. This value was obtained by observing the preform in crossed polarizers according to the number of interference fringes (Figure 4c; for a description of the method, see [19,20]). The tensile stresses in this case (0.05 GPa) were significantly lower than the estimated stresses in the preforms in our experiments (~20 GPa), but they could also cause crack propagation (see Figure 5a). In this case, the stresses were too small to cause the formation of cracks in the bulk of the glass. Therefore, for starting a crack, an initiation is required. In the BS preform in Figure 5a, crack propagation was initiated when an attempt was made to cut the preform in half with a diamond blade. In this case, Figure 5a shows the formation of a complex pattern of a large number of cracks close to annular in shape, starting in the middle part of the core and then penetrating into the reflective cladding. For comparison, consider the initiated crack propagation in preform PS1 doped with only 3 mol.% P_2O_5 with a lower stress level (see Figure 5b). With a decrease in the level of residual stresses, the pattern of formed cracks was significantly simplified in comparison with the BS preform and became more accessible for analysis. The crack shape in the cross-sections of the PS1 preform approached an ideal ring. Figure 5b demonstrates the fact that cracks propagated mainly perpendicularly to tensile stress lines.

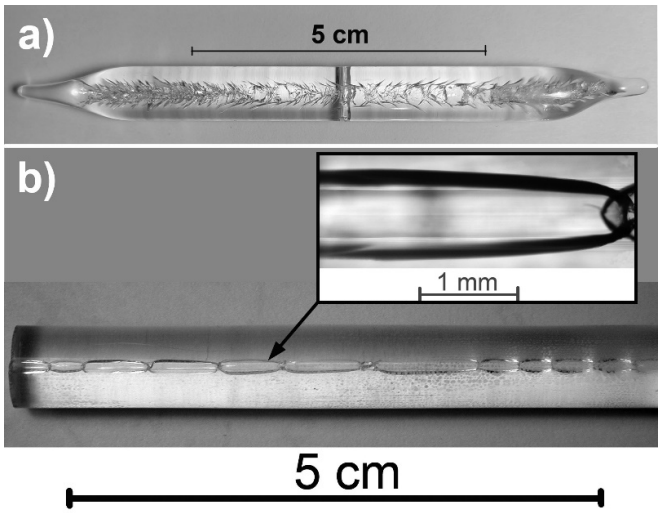

Figure 5. (**a**) Picture of the BS preform after stressed core cracking in the process of preform cutting with a diamond blade. The tensile stress in the core was 50 MPa, and the crack propagation velocity was >1 m/s. (**b**) For comparison, picture of cracking of the PS1 preform with lower residual tensile stress (preform with low level of P_2O_5 dopant). The crack propagation velocity was ~2×10^{-3} mm/s. The inset shows a section of the preform on a larger scale. Here, one can see the core of the preform surrounded by an ellipsoidal crack.

However, in the heated preform (Figure 3), a change in the RI of the core was observed, which indicates a compressed state of the core. The features of the formation of cracks in glass in this case are considered below. First, let us discuss a physical mechanism for the formation of high pressure in the core of the preform during its manufacture. For the appearance of compressive stresses in the core, it was necessary that, upon cooling, the core material density decreased and, accordingly, its volume increased in the temperature range in which measurements were taken. In fact, the measurements were carried out at high temperatures during the cooling of the preform (from 2000 °C); hence, the temperature at the core–cladding interface first achieved the value of T_g for SiO_2 and then T_g for the doped core glass. It is known that, at high temperatures (on the order of T_g), the glass structure changes, and its thermophysical properties change significantly. Although there are very few detailed data on the CTE of glasses of a specific composition and their melts at high temperatures, it is known that, near the glass T_g, different compositions of silica glasses demonstrate density changes sufficient to generate high pressure in the silica preform core [2,3,21,22]. These similar properties were also demonstrated for chalcogenide glasses [23], where local jumps in CTE and density were observed near the glass transition temperature.

Therefore, it is quite possible that, during cooling, the support silica tube had already cooled below its glass transition point and solidified. Compared to doped glasses, it can be assumed that the material of a tube made of pure SiO_2 does not change its density and volume after the silica glass transition temperature. At the same time, the still melted silicate core, approaching its glass transition point in a certain temperature range, tends to increase its volume in a rigid silica tube (having a CTE lower then the CTE of pure silica glass). Thus, different glass transition temperatures of the core and cladding and a local extremum in density of doped glass can obviously lead to the formation of compressive stresses in a certain temperature range near T_g of the core glass, as well as an increase in pressure and RI. After further cooling, the density of the core would increase again, and the tensile stress in the core would be established.

Next, we consider a second question: what currently known phenomena can indicate the occurrence of compressive stresses in the core region with an amplitude of tens of gigapascals? It is known that the difference in the coefficients of thermal expansion (CTE) between the cladding glass (α_1) and the core material (α_2) during sample cooling leads to

the formation of annular cracks if $\alpha_2 > \alpha_1$ (e.g., in Figure 2b (GS) **1**, Figures 5 and 6d) and to the formation of radial cracks if $\alpha_1 > \alpha_2$ [24].

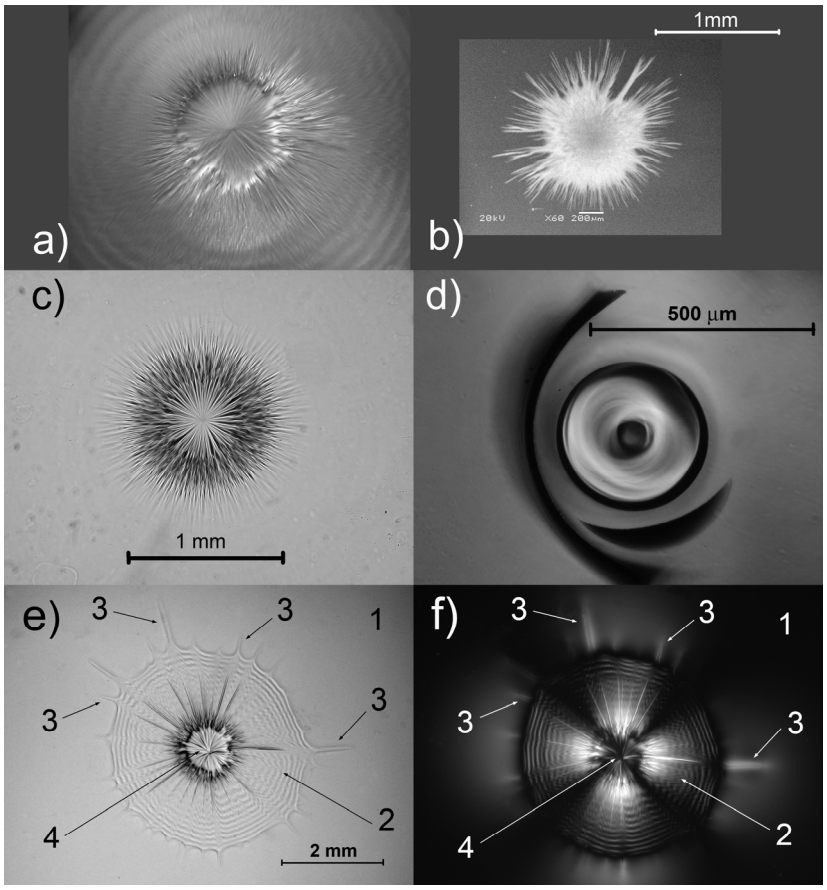

Figure 6. Pictures of polished cross-sections of fiber preforms with radial cracks (**a**–**f**), and with annular cracks (**d**). (**a**) Cross-section of an aluminosilicate preform taken by optical microscope; (**b**) SEM picture of the same preform, showing the distribution of the core glass; (**c**) cross-section of a germanosilicate preform taken by optical microscope; (**d**) picture of the phosphosilicate preform with annular cracks; (**e**) cross-section of Al + Ge preform (2.5 mol.% Al_2O_3 and 1.0 mol.% GeO_2, 11 layers of inner cladding); (**f**) the same picture taken with crossed polarizers for better crack visibility. The scales in (**a**,**b**) and (**e**,**f**) are the same. 1—support tube; 2—inner cladding; 3—some of the cracks penetrating into the support tube; 4—core of the fiber preform.

We propose to pay attention to a well-known phenomenon: the formation of so-called "stars" in the cross-sections of fiber preforms based on silica glass cores doped with relatively high concentrations of germania or alumina [10,11,25–27]. Example photographs of cross-sections of such preforms are shown in Figure 6.

It is possible that mechanism of "star" formation could be as follows: due to the high values of compressive stress in still liquid core glass, cracks appear in the cladding (the cladding is no longer liquid at the certain temperature) directed mainly along the radius of the preform, which are then immediately filled with the substance of the liquid core. The branching of "star rays" observed in Figure 6b is similar to the branching of cracks in glasses [14,24]. This fact can serve as an additional argument in favor of the crack origin of "starbursts". Since the glass transition temperature of the core (silica glass with a relatively high level of GeO_2 or Al_2O_3 dopants) is lower than the glass transition temperature of SiO_2, this may explain why cracks occur in SiO_2 cladding cracks, before being filled with core material. This assumption is supported by the cross-sectional view of the GS preform with radial and annular cracks (Figure 2b (GS)). Obviously, the star-shaped core (with rays along the radius) was formed during the manufacture of the preform at high temperature,

indicating the compressive stress of the core material. An annular crack appeared around the core and partially separated the core from the cladding when the cold preform was cut. This crack was a consequence of the tensile stress of the core at room temperature.

The previously proposed model in [25] describes this phenomenon as a function of the instability of the interface during the flow of fluids with significantly different viscosities. A viscoelastic model of "starburst" formation was suggested in [10], assuming the folding of a single core layer during the collapse of the preform for describing the formation of stars in the core of preforms of optical fibers. However, in the frames of these models, the formation of pressure at the level of tens of GPa in the fiber core region cannot be explained. Moreover, it is known that the different rays of the "stars" in the cores of the preforms, as a rule, have different lengths. In a number of preforms, these rays not only penetrate the entire inner cladding, but also penetrate into the support tube made of F-300 silica (Heraeus) (see Figure 6e,f). Such a phenomenon also cannot be explained by the existing models. Furthermore, this fact is a direct indication that, in this case, we are dealing with the propagation of cracks through the inner cladding and their penetration into the glass of the support tube. The existence of cracks implies the presence of high enough tensile stresses in the region of the core of the preform, as noted at the beginning of this section.

We would also like to point out that, despite the extensive experimental experience of some authors with fiber-optic technologies, the formation of "stars" in phosphorus-doped fiber preform has not been observed. To the best of our knowledge, there is no such information in the literature. On this basis, within the framework of the proposed model, it can be concluded that, during the manufacturing of phosphosilicate fiber preforms, the core compression stresses are insufficient to cause cracking in the preform cladding.

5. Conclusions

The thermal radiation angular diagrams at a high temperature (~2000 °C) demonstrated an apparent difference in the intrinsic radiation intensity from the area of the core–cladding interface of optical fiber preforms for two orthogonal polarizations. From this intensity difference, the liquid core glass RI n_2 was estimated for PS and GS preforms. The lower estimates were n_2 = 1.64 (PS preform) and n_2 = 1.75 (GS preform). These values correspond to core pressures of ~15 GPa and ~30 GPa [12]. The presence of radial cracks in the cladding of the GS preform after cooling and the absence of such cracks in the PS preform could be associated with lower peak pressures in the PS preform core compared to the GS preform core.

The results of this study provide an instrument to gain a more in-depth understanding of the physical phenomena in the preform core region during its fabrication, and they can help to better control the MCVD process. In particular, direct measurement of the core RI during the manufacturing process of the fiber preform makes it possible to predict the appearance of defects. A higher core RI results in a higher probability of "star" formation in the preform core with a corresponding increase in fiber optical losses. Generally, the method considered herein for directly obtaining information about fiber preforms in the process of fabrication opens up additional possibilities for improving the quality of optical fibers drawn from these preforms.

The results obtained may also be of interest for other technological processes of fiber preform fabrication. In addition, the knowledge of the refractive index and of the pressure in the core glass can also be useful for controlling the fiber drawing process, e.g., in the melt-in tube (MIT) technology [28].

The data obtained allowed us to propose a new model for "star" formation in the MCVD preform core. The model considers "starbursts" as radial cracks in the preform cladding and is consistent with the following experimental facts: (1) the hydrostatic pressure of the melted preform core can be close to the failure threshold of the silica glass; (2) the cracks penetrate from the core region into the preform support tube.

The demonstration of gigapascal pressures in fabricating silica fiber preforms opens up new possibilities for achieving high pressures in science and technology.

Author Contributions: Conceptualization, G.B. and I.B.; methodology, G.B., A.K., V.V. and I.B.; formal analysis, G.B.; investigation, G.B., A.K., V.V., M.Y. and I.B.; resources, A.K., V.V., M.Y., A.U. and V.T.; writing—original draft preparation, G.B.; writing—review and editing, G.B., V.T., A.U. and I.B.; visualization, G.B.; supervision, I.B.; project administration, G.B.; funding acquisition, I.B. All authors read and agreed to the published version of the manuscript.

Funding: This research was supported by the Russian Science Foundation (grant No. 19-12-00361).

Institutional Review Board Statement: Not applicable.

Informed Consent Statement: Not applicable.

Data Availability Statement: The data supporting the findings of this study are available within the article.

Acknowledgments: The authors thank V.F. Khopin for useful discussions. The authors are also grateful to V.V. Valuev for his help in carrying out the experiments.

Conflicts of Interest: The authors declare no conflict of interest.

References

1. Shelby, J.E. Chapter 14 Compositions and Properties of Commercial Glasses. In *Introduction to Glass Science and Technology*; Royal Society of Chemistry: London, UK, 2005; pp. 262–273.
2. Bruckner, R. Properties and structure of vitreous silica. *J. Non-Cryst. Solids* **1970**, *5*, 123–175. [CrossRef]
3. Mysen, B.; Richet, P. *Silica in Silicate Glasses and Melts*; Elsevier: Amsterdam, The Netherlands, 2019; pp. 147–163.
4. Waxler, R.M.; Cleek, G.W. The Effect of Temperature and Pressure on the Refractive Index of Some Oxide Glasses. *J. Res. Natl. Bur. Stand.-A Phys. Chem.* **1973**, *77A*, 756–773. [CrossRef] [PubMed]
5. Susa, M.; Kamijo, Y.; Kusano, K.; Kojima, R. A predictive equation for the refractive indices of silicate melts containing alkali, alkaline earth and aluminium oxides. *Glass Technol.* **2005**, *46*, 55–61.
6. Yablon, A.D. Optical and mechanical effects of frozen-in stresses and strains in optical fibers. *IEEE J. Sel. Top. Quantum Electron.* **2004**, *10*, 300–311. [CrossRef]
7. Bufetova, G.A.; Kashin, V.V.; Rusanov, S.Y.; Seregin, V.F.; Tsvetkov, V.B. Measurement of the refractive index of an Er^{3+}: YAG crystal melt. *J. Appl. Phys.* **2020**, *127*, 035104. [CrossRef]
8. Bufetova, G.A.; Kashin, V.V.; Rusanov, S.Y.; Seregin, V.F.; Tsvetkov, V.B. Determination of sapphire crystal melt refractive index in visible range. *J. Cryst. Growth* **2021**, *575*, 126355. [CrossRef]
9. Malinin, A.A.; Zlenko, A.S.; Akhmetshin, U.G.; Semjonov, S.L. Furnace Chemical Vapor Deposition (FCVD) method for special optical fibers fabrication. *Proc. SPIE* **2011**, *7934*, 793418. [CrossRef]
10. McNamara, P.; Lyytikainen, K.J.; Ryan, T.; Kaplin, I.J.; Ringer, S.P. Germanium-rich "starburst" cores in silica-based optical fibres fabricated by modified chemical vapour deposition. *Opt. Commun.* **2004**, *230*, 45–53. [CrossRef]
11. Dhar, A.; Das, S.; Maiti, H.S.; Sen, R. Fabrication of high aluminium containing rare-earth doped fiber without core–clad interface defects. *Opt. Commun.* **2010**, *283*, 2344–2349. [CrossRef]
12. Zha, C.S.; Hemley, R.J.; Mao, H.K.; Duffy, T.S.; Meade, C. Acoustic velocities and refractive index of $Si0_2$ glass to 57.5 GPa by Brillouin scattering. *Phys. Rev. B* **1994**, *50*, 13105–13112. [CrossRef] [PubMed]
13. Timoshenko, S.P.; Goodier, J.N. *Theory of Elasticity*; McGraw-Hill: New York, NY, USA, 1970; pp. 65–71.
14. Scholze, H. *Glass: Nature, Structure, and Properties*; Springer Inc.: New York, NY, USA, 1991; pp. 258, 262–267.
15. Shelby, J.E. Chapter 9 Mechanical Properties. In *Introduction to Glass Science and Technology*; Royal Society of Chemistry: London, UK, 2005; p. 191.
16. Bogatyrjov, V.A.; Bubnov, M.M.; Dianov, E.M.; Makarenko, A.Y.; Rumyantsev, S.D.; Semjonov, S.L.; Sysoljatin, A.A. High-strength hermetically tin-coated optical fibers. In Proceedings of the Optical Fiber Communication Conference, San Diego, CA, USA, 18 February 1991; Optica Publishing Group: Washington, DC, USA, 1991; p. WL9.
17. Bogatyrjov, V.A.; Dianov, E.M.; Rumjantsev, S.D.; Makarenko, A.Y.; Semjonov, S.L.; Sysoljatin, A.A. Super-high-strength hermetically metal-coated optical fibres. *Sov. Light. Commun.* **1991**, *1*, 227–234.
18. Aben, H.; Guillemet, C. *Photoelasticity of glass*; Springer: Berlin/Heidelberg, Germany, 1993; pp. 216–227.
19. Saunders, M.J. Determination of the stress in optical fibers by means of a polariscope. *Rev. Sci. Instrum.* **1976**, *47*, 496–500. [CrossRef]
20. Shibata, N.; Kawachi, M.; Edahiro, T. Refractive-index profiling of preform rods by a photoelastic method: Application to VAD single-mode fiber performs. *Appl. Opt.* **1982**, *21*, 3507–3510. [CrossRef] [PubMed]
21. Dichte von Coenen, M. "Schlierengläsern" bei hohen Temperaturen. *Glastechn. Ber.* **1966**, *39*, 7.
22. Leko, V.K.; Mazurin, V.O. *Svoistva Kvartsevogo Stekla (Properties of Silica Glass)*; Nauka: Leningrad, Russia, 1985; pp. 44–55.
23. Tver'yanovich, Y.S.; Ugolkov, V.L.; Il'chenko, O.V. Smeared first-order phase transition in chalcogenide melts. *J. Non-Cryst. Solids* **1999**, *256–257*, 78–82. [CrossRef]

24. Von Kerkhof, F. Bruchentstehung und Bruchausbreitung im Glas. In *Book Glastechnische Fabrikationsfehler*, 4th ed.; Brückner, R., Jebsen-Marwedel, H., Eds.; Springer: Berlin/Heidelberg, Germany; p. 545, Figures 21 and 27.
25. Biryukov, A.S.; Dianov, E.M.; Kurkov, A.S.; Devyatykh, G.G.; Gur'yanov, A.N.; Gusovskii, D.D.; Kobis, S.V. Core-cladding interface instability as one of the source of additional losses in high doped optical fibers. In Proceedings of the European Conference on Optical Communication (IEEE Cat. No. 96TH8217), Oslo, Norway, 19 September 1996; Telenor: Kjeller, Norway; Volume 2, paper TuP.02, 225.
26. Paul, M.; Kir'yanov, A.; Barmenkov, Y.; Pal, M.; Youngman, R.; Dhar, A.; Das, S. Phase-separated alumina–silica glass-based erbium-doped fibers for optical amplifier: Material and optical characterization along with am-plification properties. *Fibers* **2018**, *6*, 67. [CrossRef]
27. Bubnov, M.M.; Semjonov, S.L.; Likhachev, M.E.; Dianov, E.M.; Khopin, V.F.; Salganskii, M.Y.; Guryanov, A.N.; Fajardo, J.C.; Kuksenkov, D.V.; Koh, J.; et al. On the origin of excess loss in highly GeO_2-doped single-mode MCVD fibers. *IEEE Photonics Technol. Lett.* **2004**, *16*, 1870–1872. [CrossRef]
28. Zhang, Y.; Qian, G.; Xiao, X.; Tian, X.; Chen, Z.; Zhong, J.; Ma, Z.; Guo, H.; Xu, S.; Yang, Z.; et al. A yttrium aluminosilicate glass fiber with graded refractive index fabricated by melt-in-tube method. *J. Am. Ceram. Soc.* **2018**, *101*, 1616–1622. [CrossRef]